J Solid State Electrochem (2006) 10: 479–487
DOI 10.1007/s10008-005-0022-x

ORIGINAL PAPER

B. A. Khorkounov · H. Näfe · F. Aldinger

Relationship between the ionic and electronic partial conductivities of co-doped LSGM ceramics from oxygen partial pressure dependence of the total conductivity

Received: 2 January 2005 / Revised: 20 May 2005 / Accepted: 23 May 2005 / Published online: 28 July 2005

Abstract $La_{0.8}Sr_{0.2}Ga_{0.85-x}Mg_{0.15}Co_xO_{3\pm\delta}$- materials (further cobalt-doped LSGM), where x varied from 0 to 0.20, were synthesized by means of the conventional powder route. The total conductivity of the $La_{0.8}Sr_{0.2}Ga_{0.85-x}Mg_{0.15}Co_xO_{3\pm\delta}$ samples was measured as a function of temperature (400–900 °C) and oxygen partial pressure ($1\times10^{-1} \le p_{O_2}[\mathrm{Pa}] \le 1\times10^{5}$) by means of the impedance technique. The values of the oxygen ionic and the hole conductivities were determined from non-linear regression of the oxygen partial pressure dependence of the total conductivity. It was shown that the substitution of gallium by cobalt in the LSGM results in increasing either the oxygen ionic or the hole conductivity, although the increase of the hole conductivity due to the doping by cobalt is more significant than the increase of the oxygen ionic conductivity. The hole conductivity of the selected compositions was studied by oxygen permeation- and Hebb–Wagner-polarization measurements.

Keywords Lanthanum gallate · Cobalt doping · Electrical conductivity · Ionic conductivity · Hole conductivity

Introduction

$La_{1-x}Sr_xGa_{1-y-z}Mg_yCo_zO_{3\pm\delta}$ (LSGM), doped by cobalt is reported to be a mixed conductor with a relatively high electrical conductivity [1–5]. Ishihara [6] has claimed that such materials could also be used as possible electrolytes for solid oxide fuel cells (SOFC). The application of cobalt-doped LSGM, as a promising material for gas separation membranes is conceivable [7]. These two proposed application areas of cobalt-doped LSGM are based on two contradictory tendencies: possible electrolytes for SOFC request a predominant ionic conductivity, whereas materials for gas separation membrane should have a considerable part of the electronic conduction. The knowledge about the relationship between the ionic and the electronic conductivities of cobalt-doped LSGM is still contradictory. This might be due to the difficulty of experimentally determining and clearly separating the oxygen ionic and electronic conductivities of such a mixed conductor. In the present work, a contribution towards this problem is to be made by characterizing the conduction properties of cobalt-doped LSGM using impedance measurements under varying oxygen atmospheres. The influence of the cobalt doping concentration on the relationship between the ionic and the electronic conductivities was of particular interest. The selected specimens were also investigated by means of oxygen permeation and Hebb–Wagner-polarization measurements to allow comparison of results obtained by different measuring techniques.

B. A. Khorkounov (✉)
Leibniz Institute for Solid State and Materials Research,
PF 27 00 16, 01171 Dresden, Germany
E-mail: B.Khorkounov@ifw-dresden.de
Tel.: +49-351-4659749
Fax: +49-351-4659541

H. Näfe · F. Aldinger
Pulvermetallurgisches Laboratorium,
Max-Planck-Institut für Metallforschung,
Heisenbergstraße 3, 70569 Stuttgart, Germany

Theoretical consideration

Defect chemistry of cobalt-doped LSGM. Oxygen-ionic and electronic conductivity

In LSGM, the oxygen vacancies are formed as a consequence of the charge balance due to the substitution of lower valent cations (i.e. Sr^{2+} and Mg^{2+}) into La^{3+} and Ga^{3+} positions, respectively:

$$V'''_{La} + V'''_{Ga} + 3V^{\bullet\bullet}_{O} + MgO + SrO \rightleftarrows Sr'_{La} + Mg'_{Ga} + 2O^{\times}_{O} + V^{\bullet\bullet}_{O} \quad (1)$$

which leads to considerable increase of the electrical conductivity [8]. The additional substitution of Co-ions

into Ga^{3+} sites can lead to a further increase of the concentration of oxygen vacancies if cobalt exists in the Co^{2+} state:

$$V'''_{Ga} + 1.5V^{\bullet\bullet}_{O} + CoO \rightleftarrows \quad Co'_{Ga} + O^{\times}_{O} + \frac{1}{2}V^{\bullet\bullet}_{O} \tag{2}$$

Cobalt, however, may adopt different valence states. If cobalt exists as three-valent cation, there is no effect on the oxygen vacancy concentration. Although the oxidation of three-valent cobalt cations to a four-valent form can cause a decrease in the oxygen vacancy concentration:

$$2Co^{\times}_{Ga} + V^{\bullet\bullet}_{O} + \frac{1}{2}O_2 \rightleftarrows \quad O^{\times}_{O} + 2Co^{\bullet}_{Ga} \tag{3}$$

The valence state of cobalt is mainly determined by the electron concentration in the solid and, thus, by the equilibrium of the solid with the oxygen containing gas phase. At high PO_2 it holds that:

$$\frac{1}{2}O_2 + V^{\bullet\bullet}_{O} \rightleftarrows \quad O^{\times}_{O} + 2h^{\bullet}, \tag{4}$$

At low oxygen activities, oxygen is removed from the crystalline lattice and electrons are generated for electroneutrality reasons:

$$O^{\times}_{O} \rightleftarrows \quad V^{\bullet\bullet}_{O} + 2e' + \frac{1}{2}O_2, \tag{5}$$

For $La_{0.8}Sr_{0.2}Ga_{0.85\text{-}x}Mg_{0.15}Co_xO_{3\pm\delta}$, the following electroneutrality condition has to be taken into account:

$$2[O''_i] + [e'] + [Sr'_{La}] + [Mg'_{Ga}] + [Co'_{Ga}] = [h^{\bullet}] + 2[V^{\bullet\bullet}_{O}] + [Co^{\bullet}_{Ga}]. \tag{6}$$

If it is assumed that the concentration of vacancies is constant under the experimental conditions:

$$([Sr'_{La}] + [Mg'_{Ga}] + [Co'_{Ga}]) \cong 2[V^{\bullet\bullet}_{O}] = \text{const.} \tag{7}$$

Thus, the concentration of the oxygen vacancies should be independent on oxygen partial pressure and controlled only by the doping concentrations of Sr^{2+}, Mg^{2+} and Co^{2+} ions and the ionic conductivity is expected to be constant. It follows from Eq. 4 that:

$$\sigma_p = \sigma^0_p \cdot p^{1/4}_{O_2}. \tag{8}$$

Here, σ^0_p is the p-type electronic conductivity at oxygen partial pressure of 1 bar.

In the limiting case (7) of the electroneutrality condition (6), the concentration of the electrons is negligibly small in comparison with that of the holes. In view of this fact, the total conductivity σ_{tot} can be expressed as:

$$\sigma_{tot} = \sigma_{ion} + \sigma^0_p \cdot p^{1/4}_{O_2}. \tag{9}$$

Eq. 9 allows separately determining σ_{ion} and σ_p by making use of the different oxygen partial pressure dependence.

It should be mentioned that the model, discussed above, could have limitations for LSGM highly doped by cobalt, as the oxygen ions mobility in such materials can be p_{O_2}-dependent [9, 10].

Oxygen permeation measurements and Hebb–Wagner-polarization technique

The hole conductivity of the selected specimens was additionally studied by the oxygen permeation and Hebb–Wagner-polarization technique in order to verify the model used for determination of the ionic and the hole conductivities from p_{O_2}-dependence of the total conductivity.

In a mixed oxide ionic-electronic conductor the difference in oxygen chemical potential at the two surfaces results in an oxygen permeation flux. This oxygen current can be expressed by the following equation:

$$I = \frac{RTS}{FL}\sigma_{ion}\ln\frac{\left(1+\frac{\sigma''_p}{\sigma_{ion}}\right)\cdot\left(1+\frac{\sigma'_n}{\sigma_{ion}}\right)}{\left(1+\frac{\sigma''_n}{\sigma_{ion}}\right)\cdot\left(1+\frac{\sigma'_p}{\sigma_{ion}}\right)}. \tag{10}$$

where p''_{O_2} and p'_{O_2} are the oxygen partial pressures at the oxygen-rich and oxygen-lean side of the permeation disc, respectively, σ''_p and σ''_n are the p- and n-electronic conductivities at $p_{O_2} = p''_{O_2}$, σ'_p and σ'_n the p- and n-electronic conductivities at $p_{O_2} = p'_{O_2}$, R, T and F are, respectively, the gas constant, the absolute temperature and the Faraday constant; L is the pellet thickness and S stands for the area of the electrolyte the oxygen ion current is flowing through. If the oxygen partial pressure fulfils the following condition: $p'_{O_2} >> p_{\ominus}$; $p'_{O_2}, p''_{O_2} \cong p_{\oplus}$, implying that the n-electronic conductivity is negligibly small, the Eq. 10) can be simplified to:

$$I = \frac{RTS}{4FL}\left(\sigma''_p - \sigma'_p\right) = \frac{RTS\sigma^0_p}{FL}\left(p''^{1/4}_{O_2} - p'^{1/4}_{O_2}\right) \tag{11}$$

The principle of Hebb–Wagner-polarization method consists of using a galvanic cell with one electrode entirely blocking to the passage of oxygen ions and the other electrode being reversible. If an external voltage is applied, the steady state current flowing through the electrolyte is of electronic nature. The electronic current I_e under the blocking condition is related with the polarization voltage U by the Hebb–Wagner equation:

$$I_e = \frac{RTS}{FL}\left\{\sigma^0_p\left[1-\exp\left(\frac{FU}{RT}\right)\right] + \sigma^0_n\left[\exp\left(-\frac{FU}{RT}\right)-1\right]\right\} \tag{12}$$

In Eq. (12), σ^0_n means the n-type electronic conductivity at PO_2 of 18a.

Materials and methods

$La_{0.8}Sr_{0.2}Ga_{0.85\text{-}x}Mg_{0.15}Co_xO_{3\pm\delta}$ $(0 \le x \le 0.20)$ were synthesized by the conventional powder route. La_2O_3 (99.99%, STREM Chemicals), $SrCO_3$ (99.999%, Alfa),

Ga_2O_3 (99.99%, Alfa), $(MgCO_3)_4{\cdot}Mg(OH)_2{\cdot}5H_2O$ (99.999%, Sigma) and Co_3O_4 (99.9985%, Alfa) were used as the starting materials. The solid-state reaction was carried out in two stages. A homogeneous mixture of the starting oxides was heated up to 1150 °C at heating rate of 5 K/min and then pre-calcined at this temperature for 2 h. This pre-calcination step was required to bind Ga into the intermediate compound; otherwise unbounded Ga_2O_3 can be reduced to Ga_2O at temperatures higher than 1200 °C and evaporates from the ceramic that leads to decreasing of the ceramic density [11, 12]. After pressing the calcined powders into the pellets (625 MPa for 1 min), the samples were sintered at 1500 °C in air for 12 h (heating rate: 5 K/min; cooling rate: 2 K/min). Such time–temperature program of preparation helps to avoid the formation of pores [13]. Calcination and sintering procedures were carried out in a closed alumina crucible.

The phase composition of the sintered samples was identified by means of room temperature powder X-ray diffraction (D5000 Diffractometer, Siemens) using CuK_α radiation and by scanning electron microscopy (SEM) with additional energy-dispersive X-ray microanalysis (Stereoscan 200, Cambridge Instruments and EDAX; Model DSM 982 Gemini, Karl Zeiss, Inc., Oberkochen, Germany). For that purpose, on gold-coated and thermally etched samples were used. In addition, optical microscopy served for estimating the porosity of the ceramics.

Pellets of essential thickness and diameter were cut out from cylindrical sample. The parallel surfaces of the pellets were ground and polished with diamond paste. Platinum was applied on the flat surface of the pellets by painting. Then, the electrodes were heated at 1000 °C for 1 h. The cooling and heating rates were 5 K/min. A two electrode symmetrical cell was build by pressing of platinum meshes with platinum current leads onto the platinum electrodes. The total electrical conductivity was measured by means of impedance spectroscopy. The impedance measurements were carried out using the frequency response analyzer SI 1260 (Solartron Instruments) in combination with the potentiostat 273 A (EG&G Princeton Applied Research). Usually, the frequency range between 100 μHz and 100 kHz was covered. The AC voltage amplitude was equal to 10 mV. The experiments were carried out in the temperature interval from 400 to 900 °C. The temperature was measured by means of an EUROTHERM 902-S temperature controller and kept constant within 0.5 K. During the measurements, the oxygen partial pressure of the gas mixtures in the ambience of the samples was varied in the range 1×10^{-1}(pure argon) $\leq p_{O_2}$ [Pa] $\leq 1 \times 10^5$ (oxygen). The oxygen concentration between these two values was adjusted by pre-mixing pure argon with pure oxygen using Tylan General RO-28 mass-flow controllers.

The oxygen permeation measurements were carried out using a potentiometric/coulometric device (OXYLYT, SensoTech, Germany) within the temperature interval from 400 to 900 °C. The densified polished samples of LSGM with known dimensions were hermetically fixed by a gold ring sealing between two gas spaces having different oxygen partial pressures controlled by the "OXYLYT". The permeation current in the LSGM pellets was measured from the surface, exposed by air, to the opposite side exposed by argon.

Hebb–Wagner-polarization measurements were conducted on the sample $La_{0.8}Sr_{0.2}Ga_{0.75}Mg_{0.15}Co_{0.10}O_{3\pm\delta}$. For this purpose, the following cell was employed: -Pt-foil (blocking)/$La_{0.8}Sr_{0.2}Ga_{0.75}Mg_{0.15}Co_{0.10}O_{3\pm\delta}$/porous Pt, air (reversible) $\oplus$

The sintered sample was ground down to 1 mm thickness and placed on a Pt-foil as an ion-blocking electrode. The specimen was inserted into a heated quartz tube and the ceramic pellet was sealed onto the Pt-foil with a glass [14] in an argon atmosphere at about 740 °C. The sealing was to ensure the ion-blocking of the Pt-foil electrode. A high impedance multimeter (Keithley 6571, Keithley Instruments Inc., USA) was used to apply a constant voltage and to measure the steady-state current through the cell.

Results and discussion

Figure 1 shows the XRD diffraction patterns of $La_{0.8}Sr_{0.2}Ga_{0.85-x}Mg_{0.15}Co_xO_{3\pm\delta}$ with cobalt concentration varying from $x = 0$ to 0.20. All the synthesized LSGM compositions exhibited a cubic phase consistent with the literature [13, 15, 16]. The splitting of the cubic (110) peak into the (110) and (104) reflections of the hexagonal cell for the composition with 20 mol% Co reported in [15] was not observed here. The lattice parameters are given in Table 1. These data are in a good agreement with values reported in [13, 15–17].

It can be seen that the sample without cobalt reveals the presence of two different secondary phases, namely, $LaSrGa_3O_7$ and $LaSrGaO_4$. Cobalt seems to change the solubility limits of Sr and Mg in the $LaGaO_3$ lattice, since the XRD plot of the sample doped with 5 mol% Co does not show a presence of any secondary phases.

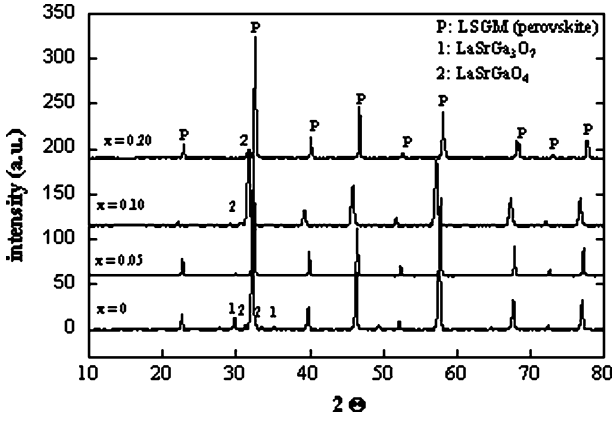

Fig. 1 Powder X-ray diffraction patterns for $La_{0.8}Sr_{0.2}Ga_{0.85-x}Mg_{0.15}Co_xO_{3\pm\delta}$ ($0 \leq x \leq 0.25$)

Table 1 Calculated cell parameters from XRD data for the compositions investigated

Composition	a (Å)	Unit cell volume (Å^3)
$La_{0.8}Sr_{0.2}Ga_{0.85}Mg_{0.15}O_{3\pm\delta}$	3.924(0)	60.44
$La_{0.8}Sr_{0.2}Ga_{0.80}Mg_{0.15}Co_{0.05}O_{3\pm\delta}$	3.909(5)	59.75
$La_{0.8}Sr_{0.2}Ga_{0.75}Mg_{0.15}Co_{0.10}O_{3\pm\delta}$	3.986(5)	63.35
$La_{0.8}Sr_{0.2}Ga_{0.65}Mg_{0.15}Co_{0.20}O_{3\pm\delta}$	3.885(1)	58.64

Secondly, cobalt improves the sinterability of LSGM-ceramics and, thus, accelerates the solid-state reaction causing more complete chemical interaction [17, 18]. The peaks of $LaSrGa_3O_7$ again appear in the diffraction patterns for $La_{0.8}Sr_{0.2}Ga_{0.75}Mg_{0.15}Co_{0.10}O_{3\pm\delta}$, their intensities, however, are significantly smaller. The sample with the highest Co content, i.e. 20 mol% Co shows additional peaks of low intensity that indicate the presence of $LaSrGaO_4$.

The average density determined by means of the Archimedes method was about 96% of the theoretical one, which was calculated on basis of XRD data.

The SEM images of $La_{0.8}Sr_{0.2}Ga_{0.85-x}Mg_{0.15}Co_xO_{3\pm\delta}$ are shown in Fig. 2a–c. It is discernible from Fig. 2a that the samples generally exhibit a high density and negligible degree of porosity. Some of the samples contain a small amount of secondary phase(s), i.e. $LaSrGa_3O_7$ that appears in the form of dark spots and $LaSrGaO_4$ that looks light-coloured (Fig. 2b, c).

$LaSrGa_3O_7$ and $LaSrGaO_4$ are reported to be the common minor phases accompanying the synthesis of LSGM [13, 19, 20]. These two phases were investigated in [20] regarded their electrical conduction properties. $LaSrGaO_4$ was found to be a low-conductive phase, while $LaSrGa_3O_7$ exhibited a relatively high electrical conductivity of about 10^{-1} S cm^{-1} of mainly p-type. As the intensity of the largest impurity peaks did not exceed 2–5% of most LSGM-phase reflections, the compositional changes in the perovskite phases due to the secondary phases segregation and the effect of minor phases on the properties of investigated LSGM ceramics were regarded to be negligible.

Figure 3 illustrates an example of characteristic Nyquist plot of the impedance data measured on $La_{0.8}Sr_{0.2}Ga_{0.75}Mg_{0.15}Co_{0.10}O_{3\pm\delta}$ at 900 °C in argon R_{dc} and R_{hf} on this plot have the meaning of the direct-current and the high frequency resistances, respectively, corresponding to the intercepts of low frequency and high frequency parts of the impedance spectra with the real (Z'-) axis of Nyquist plot. R_{hf} values, which are usually assumed to be the ohmic resistance of the electrolyte and the current leads [21], were found by extrapolation of the impedance data. The total electrical conductivity was determined from the value of R_{hf}.

Figure 4 shows the Arrhenius plot of total electrical conductivity in air of the $La_{0.8}Sr_{0.2}Ga_{0.85-x}Mg_{0.15}Co_xO_{3\pm\delta}$ ($x = 0$; 0.05; 0.10; 0.20). The results were independent of whether the samples were measured during heating or cooling. It becomes obvious that the conductivity increases with increasing cobalt concentration; the substitution by 5 mol% of Co in the Ga-positions leads to an enhancement of the total conductivity of about one order of magnitude. On further increasing the dopant concentration, the activation energy even decreases. It is interesting to note that the difference in the total conductivity values between the samples of different cobalt content is reduced with increase of temperature.

Figure 5 demonstrates the effect of the oxygen partial pressure on the total conductivity at 700 °C. It is possible to see that the slope of the plots increases with cobalt concentration.

According to [9, 10, 15, 22], cobalt remains trivalent under the conditions taken for this investigation. Hence, the vacancy concentration is expected to be independent on p_{O_2}.

Figure 6 shows fitting the experimental data to Eq. 9 for the compositions with 0; 5 and 10 mol% Co. Statistical parameters (correlation coefficients and dispersions) showing the fit quality using the model mentioned at 700 and 900 °C are cited in Table 2. The satisfactory fitting parameters confirm the adequacy of the fitting model applied.

The oxygen ionic conductivity, calculated by least square method from oxygen partial pressure dependence of total conductivity, is presented in Fig. 7 as a function of temperature. The figure shows that the substitution by cobalt seems to cause the increase in the ionic conductivity: the values of the ionic conductivity of all the cobalt substituted LSGM are higher than that for the sample without cobalt. The enhancement amounts to about one order of magnitude. The highest value of the oxygen-ionic conductivity is observed for the sample with $x = 0.10$. This means that the ionic conductivity of the composition with the highest investigated cobalt doping concentration is lower than that of the samples $x = 0.05$ and 0.10. This can be explained by a too high number of the oxygen vacancies, which can be created due to such high concentration of cobalt ions ($x = 0.20$) with a lower valence. This can lead to the oxygen vacancies association, which can result in decreasing the ionic conductivity. The suppressed ionic transport at the highest investigated cobalt concentration can be also explained by the enhanced Coulombic attraction between cobalt cations and oxygen ions causing a local ordering in the oxygen-sublattice.

The activation energy for ionic conductivity varies from 0.51 to 0.69 eV, which in good agreement with the literature data [9, 23].

The temperature dependences of the hole conductivity at p_{O_2} of 1 bar, calculated from the regression

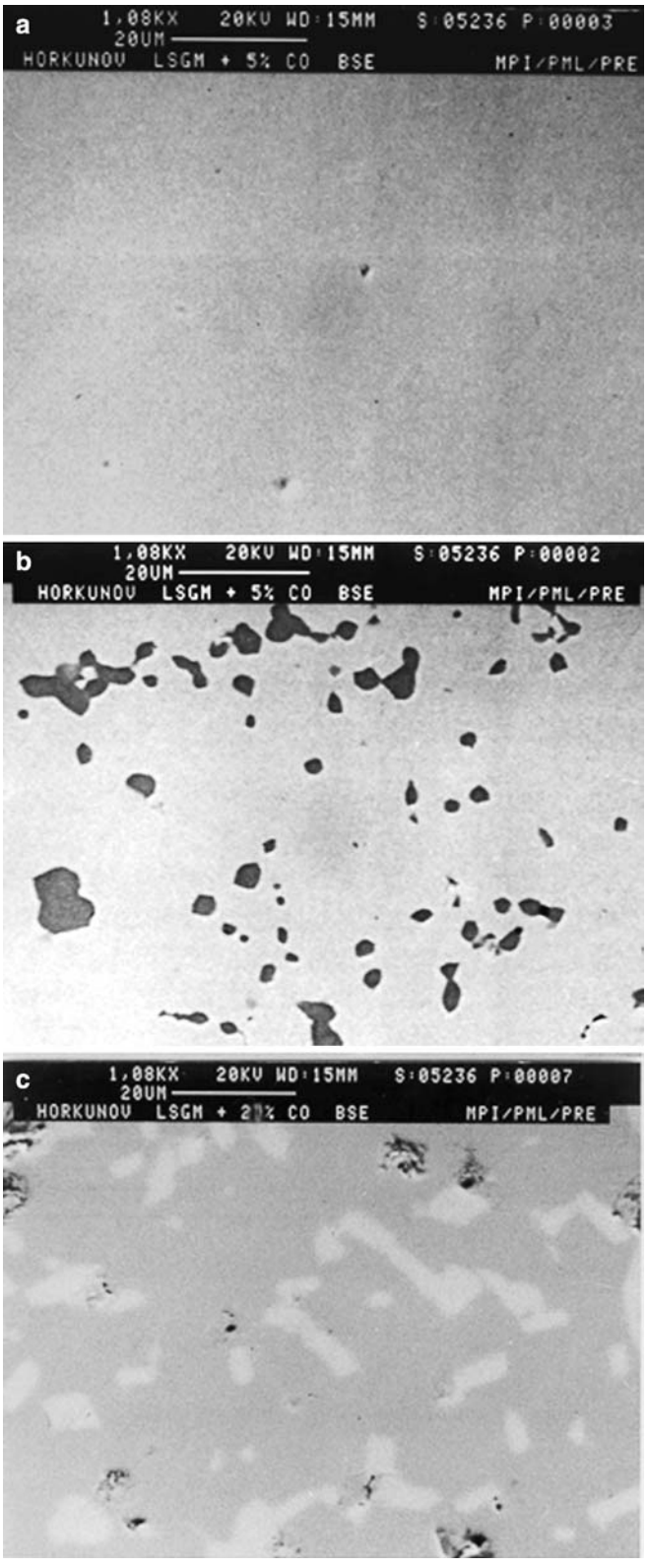

Fig. 2 SEM micrographs of sintered cobalt-doped LSGM samples (*bright inclusions* $LaSrGaO_4$; *dark inclusions* $LaSrGa_3O_7$): **a**, **b** $La_{0.8}Sr_{0.2}Ga_{0.80}Mg_{0.15}Co_{0.05}O_{3\pm\delta}$; **c** $La_{0.8}Sr_{0.2}Ga_{0.65}Mg_{0.15}Co_{0.20}O_{3\pm\delta}$

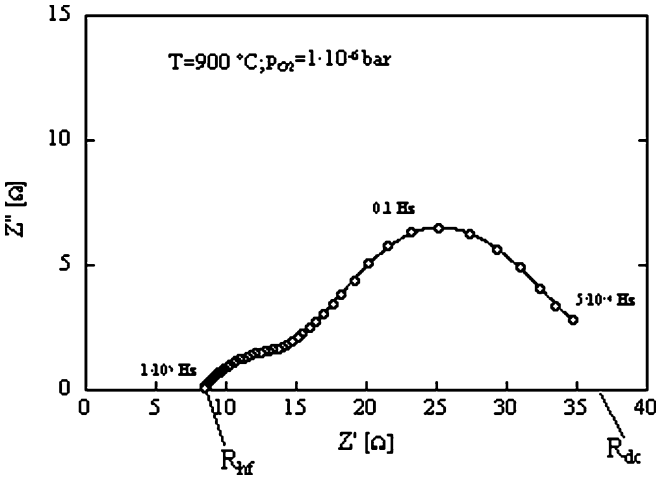

Fig. 3 An example of Nyquist plot measured on $La_{0.8}Sr_{0.2}Ga_{0.75}Mg_{0.15}Co_{0.10}O_{3\pm\delta}$ at 900 °C and $p_{O_2} = 1 \times 10^{-6}$ Pa

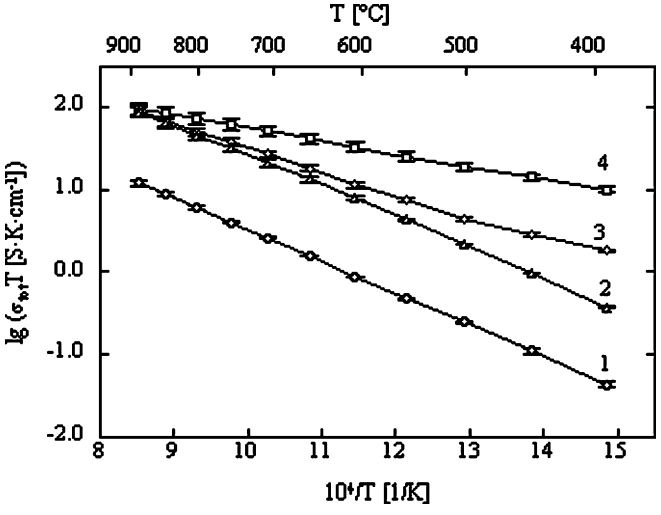

Fig. 4 Arrhenius plots of total electrical conductivity of $La_{0.8}Sr_{0.2}Ga_{0.85-x}Mg_{0.15}Co_xO_{3\pm\delta}$: *1* $x=0$; *2* $x=0.05$; *3* $x=0.10$; *4* $x=0.20$

according to Eq. 9, are shown in Fig. 8. It can be seen that the doping by cobalt results in an increase of σ_p: the higher the cobalt concentration, the higher the hole conductivity. The maximum activation energy for the hole conductivity is observed for the composition without cobalt (0.53 eV), whereas $La_{0.8}Sr_{0.2}Ga_{0.65}Mg_{0.15}Co_{0.20}O_{3\pm\delta}$ has the lowest value of the activation energy for the hole conductivity (0.15 eV). The activation energy E_a for the oxygen-ionic conductivity and the hole conductivity of $La_{0.8}Sr_{0.2}Ga_{0.85-x}Mg_{0.15}Co_xO_{3\pm\delta}$ are given in Table 3. From analysis of these data, it can be noticed that the activation energy for the hole conductivity of the sample without Co is essentially lower with respect to the data determined from the Hebb–Wagner-polarization measurements by [23, 24] for a similar compositions, but more comparable to the value

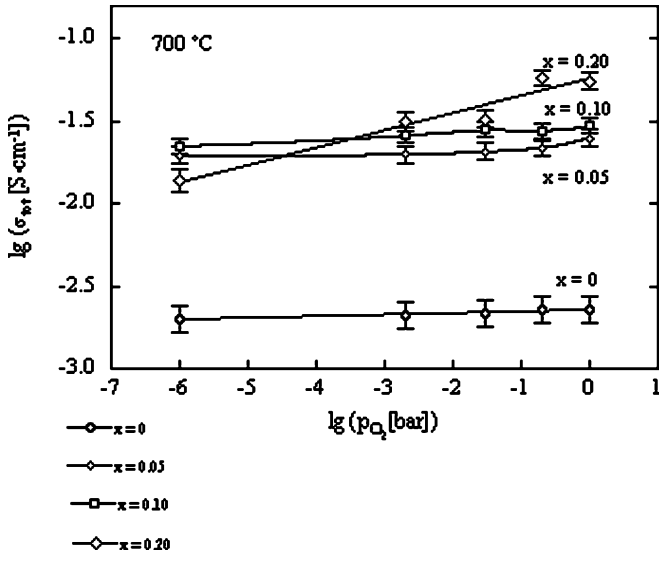

Fig. 5 Oxygen partial pressure dependence of the total conductivity for $La_{0.8}Sr_{0.2}Ga_{0.85-x}Mg_{0.15}Co_xO_{3\pm\delta}$ ($x=0$; 0.05; 0.10; 0.20) at 700 °C

obtained by Weitkamp et al. (0.66 eV) [25]. These differences can be explained by the possible limitations of the model used in this work for LSGM undoped by Co, as for this case the value of the hole conductivity is quite low. For this reason, it can be difficult to define σ_p^0 within a high accuracy, since the total conductivity of the undoped material shows a quite weak p_{O_2}-dependence.

It is obvious that the E_a value of the hole conductivity for the composition with $x=0.10$ falls out from the common sequence. Furthermore, this composition reveals the lowest value of the activation energy for the ionic conductivity. This behaviour can be explained by the fact that the lattice parameter and the cell volume of the ceramic with $x=0.10$ are larger than those of the other investigated compositions, which is visible from Fig. 1 and also from Table 1. This can influence the charge transport mechanism. According to [15, 26], increase of the lattice volume and of the free volume causes faster ionic transport. This suggestion is confirmed by the fact that LSGM doped with 10 mol% Co exhibits the highest oxygen-ionic conductivity. The activation energy for the hole conductivity of this composition exceeds those values for the other investigated Co-doped LSGM, as the hole mobility reveals the opposite dependence on the lattice volume than the oxygen ions mobility due to the small-polar on mechanism of the p-type electronic conduction [27]. Generally, both activation energies with the exception of the values for $La_{0.8}Sr_{0.2}Ga_{0.75}Mg_{0.15}Co_{0.10}O_{3\pm\delta}$ decrease with increasing cobalt concentration.

Comparing Figs. 7 and 8, it is possible to see that both of the partial conductivities, i.e. oxygen ion and hole conductivities are increased due to the cobalt doping. Nevertheless, the increase of the hole conductivity due to the cobalt substitution is more significant

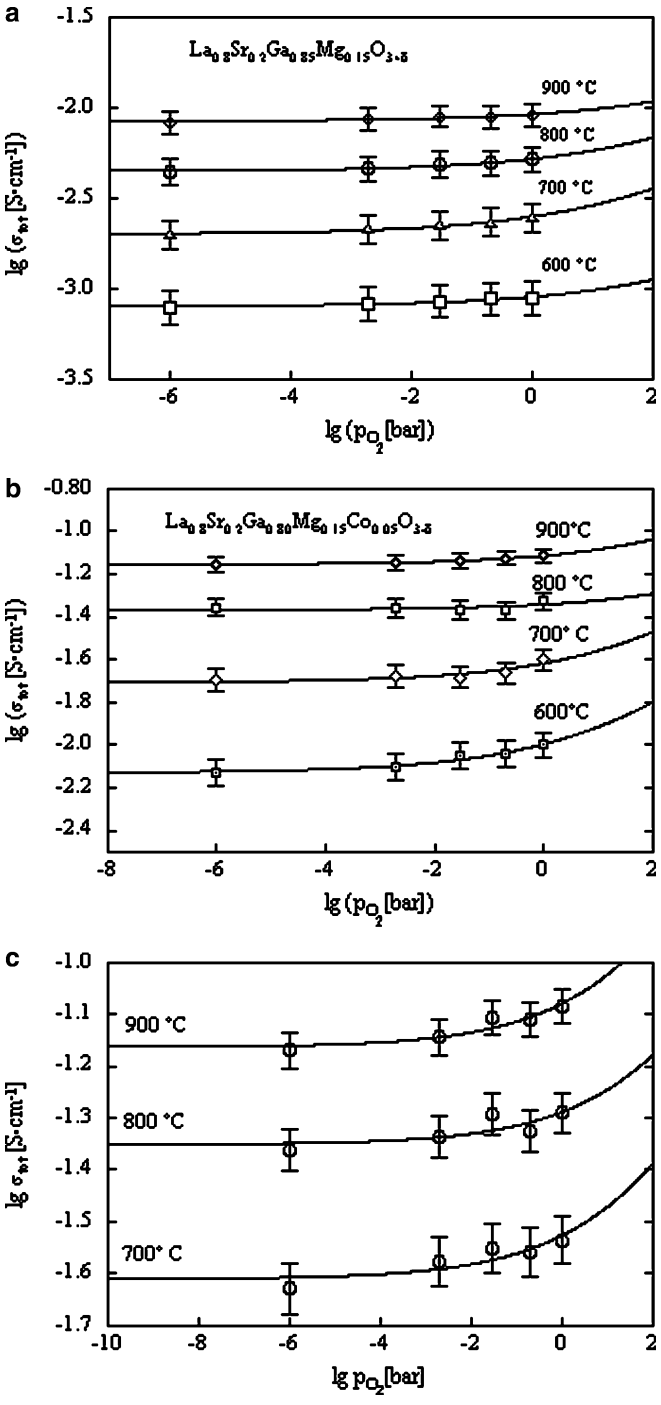

Fig. 6 The result of fitting oxygen partial pressure dependence of σ_{tot} for $La_{0.8}Sr_{0.2}Ga_{0.85-x}Mg_{0.15}Co_xO_{3\pm\delta}$ according to Eq. 9: **a** $x=0$; **b** $x=0.05$; **c** $x=0.10$

than that of the oxygen ionic conductivity. The oxygen ion and the hole conductivities are presented in Fig. 9 as a function of the cobalt concentration at 900 °C. These values, determined in present work, are compared in Fig. 9 with the values of the hole and ionic conductivities of $La_{0.8}Sr_{0.2}Ga_{0.8}Mg_{0.2-x}Co_xO_{3\pm\delta}$ from the work of Ishihara et al. [9]. The substitution of 5 mol% of Co into the Ga sites causes the increase of the ion

Table 2 Statistical parameters of the fitting using the model Eq. 9 for 700 and 900 °C

Composition	T (°C)	$-\lg\ \sigma_{ion}$ (S cm^{-1})	$-\lg\ \sigma_p^0$ (S cm^{-1})	R, correlation coefficient
$La_{0.8}Sr_{0.2}Ga_{0.85}Mg_{0.15}O_{3\pm\delta}$	900	$2.05\pm1\times10^{-4}$	2.86 ± 0.05	0.9804
	700	$2.33\pm0.00(2)$	3.29 ± 0.08	0.9502
$La_{0.8}Sr_{0.2}Ga_{0.80}Mg_{0.15}Co_{0.05}O_{3\pm\delta}$	900	$1.15\pm0.00(3)$	2.38 ± 0.10	0.9292
	700	1.69 ± 0.01	2.62 ± 0.10	0.9342
$La_{0.8}Sr_{0.2}Ga_{0.75}Mg_{0.15}Co_{0.10}O_{3\pm\delta}$	900	1.16 ± 0.01	1.84 ± 0.09	0.9425
	700	1.61 ± 0.02	2.29 ± 0.14	0.8870
$La_{0.8}Sr_{0.2}Ga_{0.65}Mg_{0.15}Co_{0.20}O_{3\pm\delta}$	900	1.36 ± 0.04	1.28 ± 0.09	0.9525
	700	1.87 ± 0.11	1.31 ± 0.09	0.9477

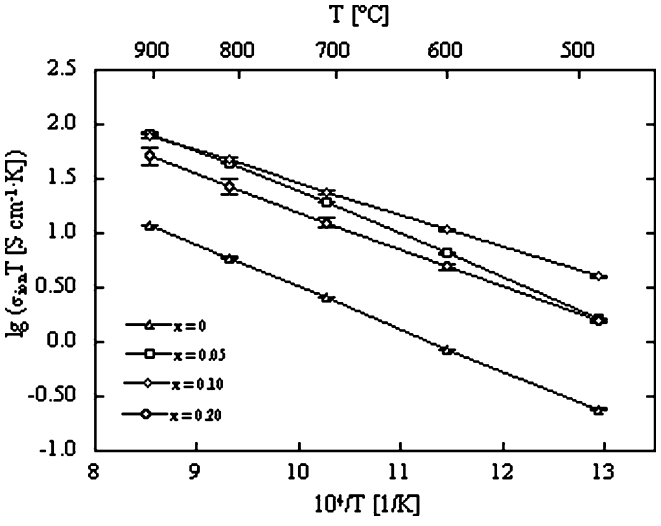

Fig. 7 Temperature dependence of the oxygen-ion conductivity of $La_{0.8}Sr_{0.2}Ga_{0.85\text{-}x}Mg_{0.15}Co_xO_{3\pm\delta}$

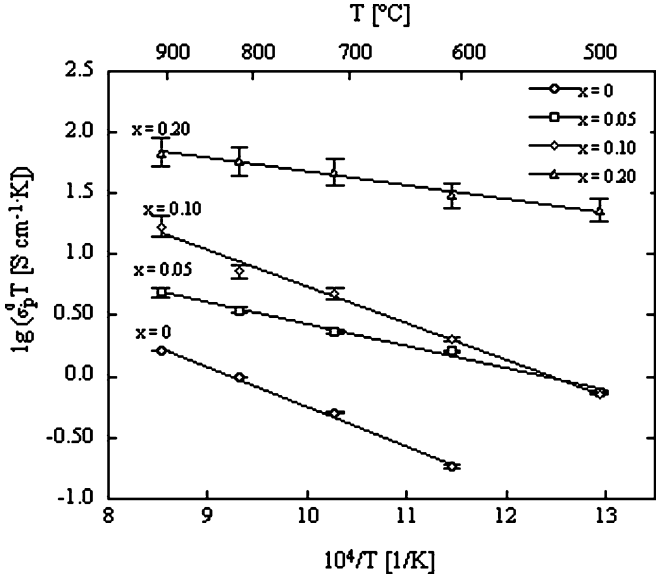

Fig. 8 Hole conductivity at $p_{O_2} = 1$ bar of $La_{0.8}Sr_{0.2}Ga_{0.85\text{-}x}Mg_{0.15}Co_xO_{3\pm\delta}$ as a function of temperature

conductivity of about one order of magnitude, but no its further significant enhancement is observed at this temperature on increasing cobalt doping concentration

Table 3 The activation energy for the oxygen-ionic and electronic conductivities of $La_{0.8}Sr_{0.2}Ga_{0.85\text{-}x}Mg_{0.15}Co_xO_{3\pm\delta}$

x in $La_{0.8}Sr_{0.2}Ga_{0.85\text{-}x}Mg_{0.15}Co_xO_{3\pm\delta}$	E_a of the ionic conductivity (eV)	E_a of the hole conductivity (eV)
0	0.69 ± 0.02	0.53 ± 0.01
0.05	0.68 ± 0.02	$0.29\pm0,01$
0.10	0.50 ± 0.01	0.51 ± 0.02
0.20	0.60 ± 0.01	0.15 ± 0.01

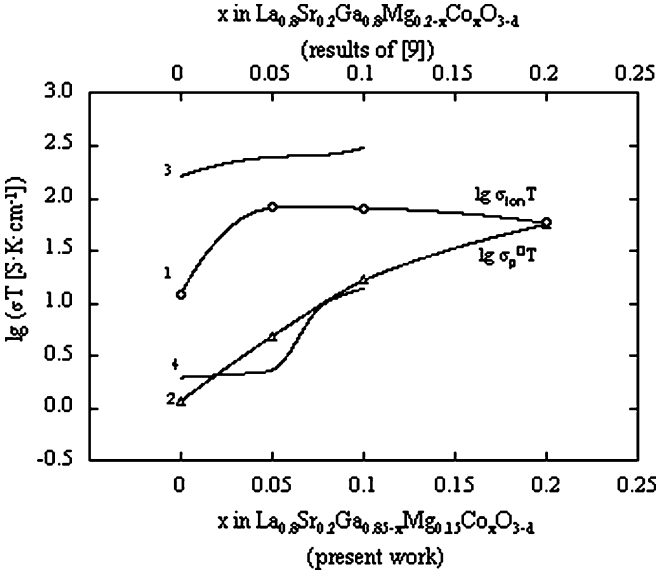

Fig. 9 Oxygen ion conductivity (σ_{ion}) and hole conductivity at $p_{O_2} = 1$ bar and at $T = 900$ °C in $La_{0.8}Sr_{0.2}Ga_{0.85\text{-}x}Mg_{0.15}Co_xO_{3\pm\delta}$ as the functions of the doping concentration of cobalt in comparison with the results of [9]: *1* $\lg\ \sigma_{ion}$ (this work); *2* $\lg\ \sigma_p^0$ (this work); *3* $\lg\ \sigma_{ion}$ [9]; *4* $\lg\ \sigma_p^0$ [9]

above 5 mol% of Co. On the other hand, the hole conductivity enhances continuously with rising the cobalt content. The hole conductivity was determined in [9] by means of the Hebb–Wagner-polarization technique. The values of the oxygen ionic conductivity were calculated there by the subtraction of the value of hole conductivity from the total conductivity. The authors of [9] observed also similar tendency of the influence of the cobalt doping on the correlation between the ionic and the hole conductivities; the increase of the hole conductivity is more significant as that of the ionic

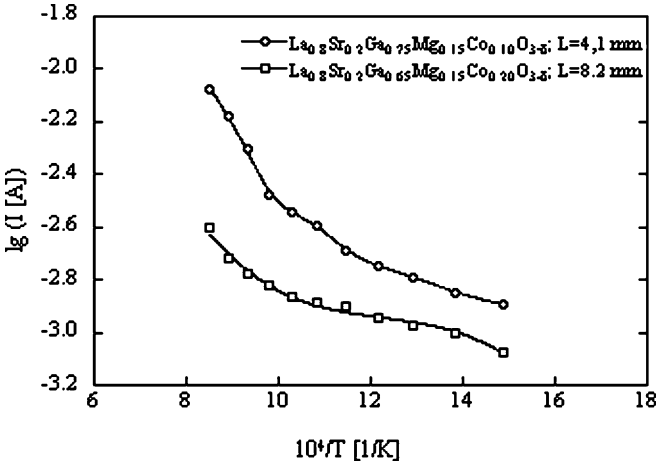

Fig. 10 Temperature dependence of the oxygen permeation current through $La_{0.8}Sr_{0.2}Ga_{0.85\text{-}x}Mg_{0.15}Co_xO_{3\pm\delta}$ ($x = 0.10$; 0.20) from air ($p''_{O_2} = 2.1 \times 10^4$ Pa) to argon $p'_{O_2} = 1$ bar

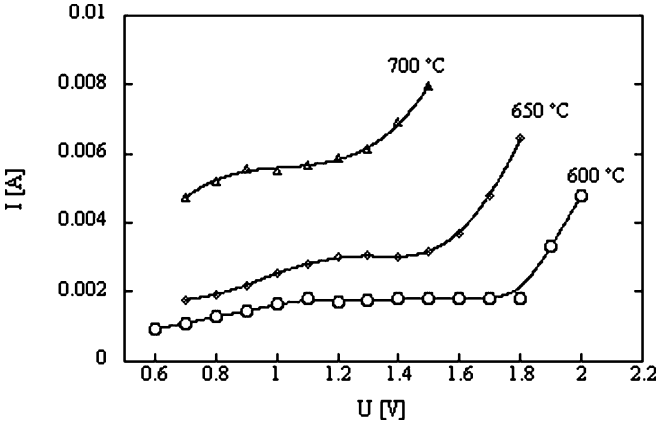

Fig. 11 Current I versus polarization voltage applied at the reversible electrode of the ion-blocking cell involving $La_{0.8}Sr_{0.2}Ga_{0.75}Mg_{0.15}Co_{0.10}O_{3\pm\delta}$ at different temperatures. The oxygen partial pressure at the reversible electrode is 0.21 bar

conductivity. The comparison between the present values of the hole conductivity at p_{O_2} of 1 bar and by Ishihara et al. [9], reveal good agreement, while the difference in values of the ionic conductivities is much more significant.

The permeation current in the samples with 10 and 20 mol% Co from air to argon is illustrated in Fig. 10 as a function of temperature. The investigated samples reveal a considerable value of the permeation current which means a high hole conductivity. The values of the permeation rate are in a good agreement with literature data for perovskite phases doped by cations of transition metals [6, 28, 29].

The electronic current-applied polarization voltage dependence obtained by Hebb–Wagner-measurements on $La_{0.8}Sr_{0.2}Ga_{0.75}Mg_{0.15}Co_{0.10}O_{3\pm\delta}$ is shown in Fig. 11. The values of σ_p^0 were determined from the nonlinear least-square fitting of the experimental data shown in Fig. 11. The latter results and the values of σ_p^0

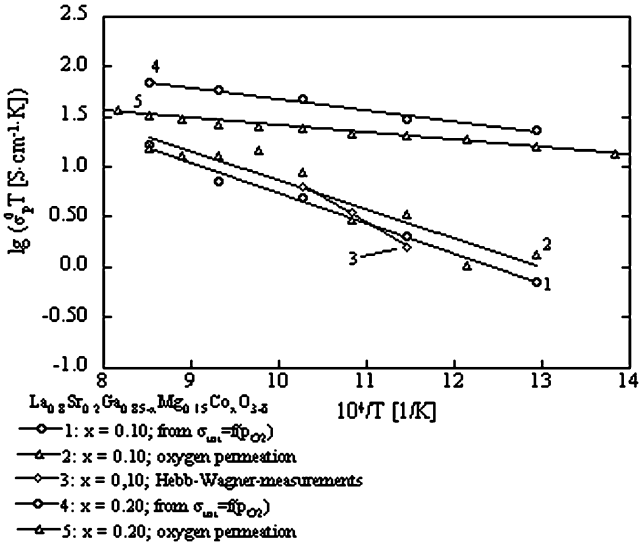

Fig. 12 The hole conductivity at $p_{O_2} = 1$ bar of $La_{0.8}Sr_{0.2}Ga_{0.85\text{-}x}Mg_{0.15}Co_xO_{3\pm\delta}$; *1* $La_{0.8}Sr_{0.2}Ga_{0.75}Mg_{0.15}Co_{0.10}O_{3\pm\delta}$ (p_{O_2}-dependence of total conductivity); *2* $La_{0.8}Sr_{0.2}Ga_{0.75}Mg_{0.15}Co_{0.10}O_{3\pm\delta}$ (oxygen permeation method); *3* $La_{0.8}Sr_{0.2}Ga_{0.75}Mg_{0.15}Co_{0.10}O_{3\pm\delta}$, Hebb-Wagner-measurements; *4* $La_{0.8}Sr_{0.2}Ga_{0.65}Mg_{0.15}Co_{0.20}O_{3\pm\delta}$ (p_{O_2}-dependence of total conductivity); *5* $La_{0.8}Sr_{0.2}Ga_{0.65}Mg_{0.15}Co_{0.20}O_{3\pm\delta}$ (oxygen permeation method)

calculated from the data of the oxygen permeation measurements using Eq. 11 are compared in Fig. 12 with the hole conductivity values determined in the present work (see also Fig. 8). It shows the satisfactory agreement between the results, measured by different experimental methods. This fact confirms indirectly the assumptions used for the fitting of the oxygen partial pressure dependences of σ_{tot} and concerning the oxygen partial pressure dependence of the hole and the oxygen-ion conductivities.

Conclusions

Depending on the cobalt content, $La_{0.8}Sr_{0.2}Ga_{0.85\text{-}x}Mg_{0.15}Co_xO_{3\pm\delta}$ ceramics ($0 \le x \le 0.20$) produced by solid-state reaction exhibit $LaSrGa_3O_7$ and $LaSrGaO_4$ as secondary phases. The total electrical conductivity investigated by means of the impedance spectroscopy increases upon substituting Ga by Co. Based on these data, the oxygen ionic and the hole conductivities were determined by assuming a non-linear regression of the oxygen partial pressure dependence of the total conductivity under the assumption that the oxygen-ionic conductivity remains independent on the oxygen partial pressure within the investigated oxygen partial pressure range. The results indicate that the both: ionic and hole conductivities are increased upon doping by cobalt. However, in case of the hole conductivity, this increase is more significant than in case of the ionic conductivity. The value of the hole conductivity enhances with the increase of cobalt content with simultaneous decrease of

its activation energy. The ionic conductivities of all the cobalt-doped samples are higher than that of the LSGM sample without cobalt. However, the increase of cobalt concentration does not mean the enhancement of the ionic conductivity: it was found that the ionic conductivity of the samples $La_{0.8}Sr_{0.2}Ga_{0.8}Mg_{0.2-x}Co_xO_{3\pm\delta}$ with $x = 0.05$ and 0.10 exceeds its of the sample with $x = 0.20$.

The values of the hole conductivity determined in the present work are in good agreement with the results of oxygen permeation measurements and Hebb–Wagner-polarization technique.

Acknowledgements The authors are especially grateful to Mrs. G. Feldhofer for technical assistance.

References

1. Ishihara T, Akbay T, Furutani H, Takita Y (1997) In:11th International conference on solid state ionics, Extended Abstracts, Honolulu, Hawaii, USA 282
2. Stevenson JW, Hasinska K, Canfield NL, Armstrong TR (2000) J Electrochem Soc 147:3213
3. Armstrong T, Prado F, Manthiram A (2001) Solid State Ionics 140:89
4. Kharton VV, Yaremchenko AA, Viskup AP, Patrakeev MV, Leonidov IA, Kozhevnikov VL, Figueiredo FM, Shaulo AL, Naumovich EN, Marques FMB (2002) J Electrochem Soc 149:E125
5. Ishihara T, Akbay T, Furutani H, Takita Y (1998) Solid State Ionics 113–115:585
6. Ishihara T, Yamada H, Arakawa H, Nishiguchi H, Takita Y (2000) Solid State Ionics 135:631
7. Kuroda K, Hashimoto I, Adachi K (2000) Solid State Ionics 132:199
8. Huang K, Petric A (1996) J Electrochem Soc 143:1644
9. Ishihara T, Ishikawa S, Yu C, Akbay T, Hosoi K, Nishiguchi H, Takita Y (2003) Phys Chem Chem Phys 5:2261
10. Ishihara T, Ishikawa S, Ando M, Nashiguchi H, Takita Y (2004) Solid State Ionics 173:9
11. Stevenson JW, Armstrong TR, Pederson LR, Li J, Lewinsohn CA, Baskaran S (1998) Solid State Ionics 113–115:571
12. Yamaji K, Negishi H, Horita T, Sakai N, Yokokawa H (2000) Solid State Ionics 135:389
13. Gorelov VP, Bronin DI, Sokolova JV, Näfe H, Aldinger F (2001) J Eur Ceram Soc 21:2311
14. Näfe H (1990) J Nucl Mater 175:67
15. Trofimenko N, Ullmann H (1999) Solid State Ionics 124:263
16. Ishihara T, Furutani H, Honda M, Yamada T, Shibayama T, Akbay T (1999) Chem Mater 11:2081
17. Polini R, Falsetti A, Traversa E (2005) DOI 10.1016/j.jeurceramsoc.2005.03.108
18. Islam NS, Davies AR (2004) J Mater Chem 14:86
19. Djurado E, Labeau M (1998) J Eur Ceram Soc 18:1397
20. Rozumek M, Majewski P, Schluckwerder H, Aldinger F, Kunstler K, Tomandl G (2004) J Am Ceram Soc 87:1795
21. Bronin DI, Yaroslavtsev IY, Näfe H, Aldinger F (2004) Electrochim Acta 49:2435
22. Long NJ, Lecarpentier F, Tuller HL (1999) J Electroceram 3:399
23. Jang JH, Choi GM (2002) Solid State Ionics 154–155:481
24. Kim JH, Yoo HI (2001) Solid State Ionics 140:105
25. Weitkamp J, Wiemhöfer HD (2002) Solid State Ionics 154–155:597
26. Yaremchenko AA, Shaula AL, Logvinovich DI, Kharton VV, Kovalevsky AV, Naumovich EN, Frade JR, Marques FMB (2003) Mater Chem Phys 82:684
27. Tsipis EV, Kharton VV, Vyshatko NV, Frade JR, Marques FMB (2005) Solid State Sci 7:257
28. Kharton VV, Yaremchenko AA, Naumovich EN (1999) J Solid State Electrochem 3:306
29. Shaula AL, Kharton VV, Marques FMB (2003) J Eur Ceram Soc 24:2631